



Science Arts & Métiers (SAM)

is an open access repository that collects the work of Arts et Métiers Institute of Technology researchers and makes it freely available over the web where possible.

This is an author-deposited version published in: <https://sam.ensam.eu>
Handle ID: <http://hdl.handle.net/10985/21618>

To cite this version :

Martin LEGRY, Frédéric COLAS, Christophe SAUDEMONT, Jean-Yves DIEULOT, Olivier DUCARME - Mixed integer quadratic programming receding horizon microgrid supervisor - In: 2019 IEEE Milan PowerTech, Italie, 2019-06 - Proceedings of 2019 IEEE Milan PowerTech - 2019

Any correspondence concerning this service should be sent to the repository

Administrator : scienceouverte@ensam.eu



Mixed integer quadratic programming receding horizon microgrid supervisor

M. LEGRY, F. COLAS, C. SAUDEMONT

Univ. Lille, Centrale Lille,
Arts et Métiers Paris Tech, HEI,
EA 2697 - L2EP
Laboratoire d'Electrotechnique et
d'Electronique de Puissance,
FRANCE
Email: Martin.legry@ensam.eu

J.Y. DIEULOT

Polytech-Lille Univ. Lille, CNRS,
Centrale Lille,
UMR 9189 - CRISAL - Centre de Recherche en
Informatique Signal et Automatique de Lille,
FRANCE

O. DUCARME

Engie Lab Laborelec
ENGIE Laborelec,
BELGIUM

Abstract—This paper proposes to optimize the real time operation of a microgrid controlled with a two-layer Model Predictive Controller supervisor. Based on the classical decomposition of control level, the proposed supervisor tracks long-term economic references from a classical economic optimization routine. The optimization problem is formulated as a Mixed Integer Quadratic Problem and uses the different power references as levers to reach this optimum and maintain the state of the microgrid within limitations. In addition, it is able to minimize the grid losses.

I. INTRODUCTION

Microgrids can be defined as a set of distributed generators, renewables or conventional ones, storage systems and loads that can operate in a coordinated manner and possibly in islanded mode. In addition, their aim is to produce locally what is needed locally, by means of local controllers. Based on conventional power system representation, the microgrid community has developed three-level structure control supervisor (see Figure 1).

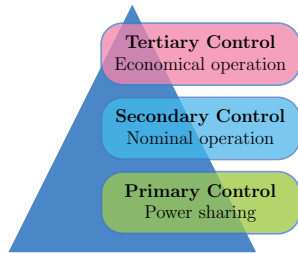


Fig. 1: Micro-grid control architecture

The primary control ensures at the faster layer the power sharing between all the active generators through well-known techniques such as classical droop control and its variants [1]. The secondary control aims to restore nominal operations of the microgrid following any fluctuation of the load or renewable sources while minimizing losses or the operating cost. Finally, the tertiary control mainly focuses on the economical optimization of the microgrid on a long-term basis. Secondary and tertiary control are also known as Power and Energy Management System (PMS and EMS) respectively. In the

latter we refer to microgrid supervisor as the combination of secondary and tertiary control layers.

There are different tools and methods to achieve the supervisor, depending on whether an optimal solution or an approached solution is desired. Among the optimal control techniques, Model Predictive Control (MPC) is one the most promising. Using two-layer MPC supervisor fits the conventional hierarchical control of microgrids previously described. On the longer timescale, an economic optimization is achieved for at least one day ahead. Model and constraints of this layer only include the slow dynamics of the equipment and economic performances of each one. On the faster timescale the cost function embeds a trajectory tracking performance, and some objectives related to the microgrid operation, such as the losses minimization or the voltage and frequency deviations. Each layer embeds a detailed model of the dynamics of interest to optimize specific criteria. However, the convergence of each objective may not be ensured. Coordinating economic constraints with real time operations is crucial for microgrid control. The problem of the cooperation between multi-layer supervisors has been discussed in [2]. It has been handled by a two-layer MPC with an intermediate module that computes reachable states, constraints and target for the lower layer based on an economical criterion. The authors of [3] proposed a formulation of a two layer MPC and addressed the problem by determining a subset of control action feasible at the higher level. Then, the lower layer solves each of the tracking problems for each feasible control action and regulate the actuators. For microgrid application, the main focus is mainly motivated to provide a solution to stochastic and uncertain forecasts, as explained in [4] and [5]. The first one is a survey on three methods to deal with the uncertainties of the renewable energy by using stochastic MPC. In [5], it is proposed to consider such stochastic optimization within the lower level and a deterministic layer at the higher. However, the models and objective functions remain the same in each layer that is to say the power balance of the microgrid and a minimization of the operating costs. In [6], the author suggested to use a multi-layer structure so that each layer

includes different model dynamics and objectives. Among the three proposed architectures, the most promising consists in a steady state optimization followed by a target correction at the lower layer side that can handle an additional task. The novelty in this paper is twofold. First, the Model Predictive Control (MPC) technique allows the supervisor to include a trajectory tracking problem into the objective function and thus to consider economic references. Second, the embedded model is able to predict the power injections at each node of the microgrid and, by upgrading the objective function, losses can be minimized.

The rest of this paper is organized as follows. In section II, the supervisor and more specifically the secondary control, its objectives and models will be detailed. To compare the conventional and novel supervisor, two simulations are presented in section III:

- Case 1: No losses minimization, the supervisor only follows the economical references,
- Case 2: The supervisor is upgraded to minimize the losses.

Finally, we will conclude on the possible improvements of this new supervisor.

II. MPC-BASED SUPERVISOR AND MICROGRID MODEL

A. Global supervisor architecture

The computation of optimal references and economic optimization of the microgrid are out of the scope of this paper, and we refer the interested reader to optimal control reviews such as [7] or unit commitment problem under uncertainties reviews [8], and finally the global architecture of the supervisor is depicted in Figure 2.

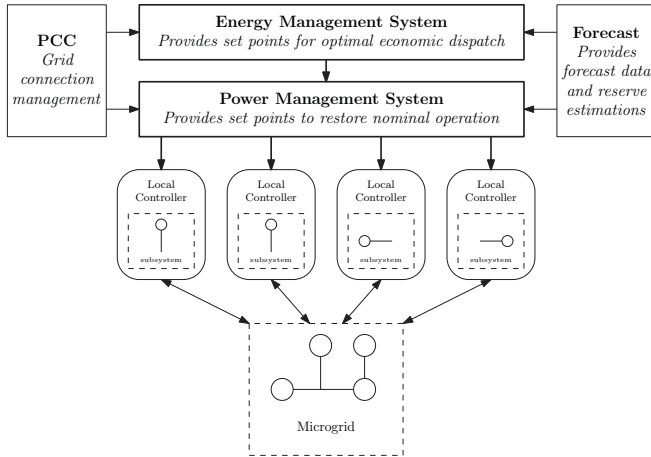


Fig. 2: Micro-grid supervisor synoptic

B. Two-layer MPC-based supervisor

To develop the proposed supervisor, we used the well-known Model Predictive Control technique which allows to capture the system future behaviour thanks to a prediction model and is able to minimize a multi-objective function with

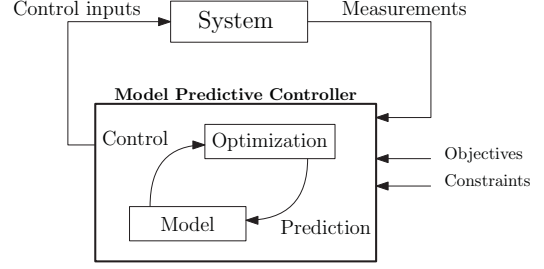


Fig. 3: Model Predictive Controller synoptic

several dynamics (see Figure 3 [6]). The model embedded in the supervisor is based on the assumptions that over the considered time scale the transient and high dynamics are not of interest, and that the system remains close to its equilibrium point. Hence, the microgrid system can be linearized and the resulting model formulated as a discrete incremental state space as follows:

$$\begin{bmatrix} x(k+1) \\ u(k) \end{bmatrix} = \begin{bmatrix} \mathbf{A} & \mathbf{B} \\ \mathbf{0} & \mathbf{I} \end{bmatrix} \begin{bmatrix} x(k) \\ u(k-1) \end{bmatrix} + \begin{bmatrix} \mathbf{B} \\ \mathbf{I} \end{bmatrix} \Delta u(k) + \begin{bmatrix} \mathbf{D} \\ \mathbf{0} \end{bmatrix} \Delta d(k)$$

$$y(k) = \begin{bmatrix} \mathbf{C} & \mathbf{0} \end{bmatrix} \begin{bmatrix} x(k) \\ u(k-1) \end{bmatrix}$$

in which $x(k)$ is the state vector at time step k , $u(k)$ the input vector at timestep k , $\Delta u(k)$ the change of input references between $(k-1)$ and (k) , and $\Delta d(k)$ the disturbance vector. Matrices \mathbf{A} , \mathbf{B} , \mathbf{D} and \mathbf{C} are obtained by the linearization of the equations of the microgrid system as detailed for the main equipment in the next section. As detailed in the introductory paragraph, the objective of the supervisor is to reach as most as possible the economic performances computed by the tertiary control. Several performance indexes can be chosen such as states of charge, produced energy or average power. In the rest of this paper we assume the upper layer uses state of charges references, and finally, the global objective function can be expressed as:

$$\min_{\Delta u} \sum_{k=1}^{N_c} \left[\alpha (\tilde{y} - y^*(k))^2 + \beta (\Delta u(k))^2 + \lambda (P_{los})^2 \right] \quad (1)$$

in which α , β , λ are the weighting factors of the trajectory deviation, the uses of levers and the line losses resp., $\tilde{y}(k)$ and $y^*(k)$ are the predicted and reference states for time k . It can be noticed that an additional objective is added in order to prevent saturation of the levers. Due to the difference of timescale between the secondary and tertiary control, a linear interpolation layer is introduced to define the references for the lower layer objective function. At last, the different levers which help to minimize the objective function will be detailed in the next sections with the modelling of the microgrid components.

C. Microgrid network model

The proposed supervisor embeds a modelling of the microgrid network in order to supervise the voltage nodes and the microgrid frequency. The traditional technique for quasi steady-state modelling of the network is based on the linearization of the power flow equations:

$$\begin{aligned} P_i &= V_i \sum_{j \in N} V_j |Y_{ij}| \cos(\delta_i - \delta_j - \theta_{ij}) \\ Q_i &= V_i \sum_{j \in N} V_j |Y_{ij}| \sin(\delta_i - \delta_j - \theta_{ij}) \end{aligned} \quad (2)$$

in which, $|V_j|$, $|V_i|$, δ_i , δ_j are the voltage magnitudes and angles resp., $|Y_{ij}|$ and θ_{ij} are the admittance matrix magnitude and angle resp. We recall that based on (3), we can derive and include the frequency in the linear model (4).

$$\begin{aligned} |Y_{ij}| &= \frac{1}{\sqrt{R_{ij}^2 + \omega^2 L_{ij}^2}} \\ \theta_{ij} &= \tan^{-1} \left(\frac{\omega L_{ij}}{R_{ij}} \right) \end{aligned} \quad (3)$$

Thus, after linearization and calculation of the Jacobian matrix ((5)), the power flow equations are modelled as follows:

$$\begin{bmatrix} \Delta V_1(k+1) \\ \vdots \\ \Delta V_i(k+1) \\ \Delta \delta_2(k+1) \\ \vdots \\ \Delta \delta_i(k+1) \\ \Delta \omega(k+1) \end{bmatrix} = \mathbf{J}^{-1} \begin{bmatrix} \Delta P_1^*(k) \\ \vdots \\ \Delta P_i^*(k) \\ \Delta Q_1^*(k) \\ \vdots \\ \Delta Q_i^*(k) \end{bmatrix} \quad (4)$$

with

$$\mathbf{J}^{-1} = \left[\begin{array}{ccc} \frac{\partial P_i}{\partial V} \bigg|_{x(k)} & \frac{\partial P_i}{\partial \delta} \bigg|_{x(k)} & \frac{\partial P_i}{\partial \omega} \bigg|_{x(k)} \\ \frac{\partial Q_i}{\partial V} \bigg|_{x(k)} & \frac{\partial Q_i}{\partial \delta} \bigg|_{x(k)} & \frac{\partial Q_i}{\partial \omega} \bigg|_{x(k)} \end{array} \right]^{-1} \quad (5)$$

and thus,

$$\begin{cases} V_i(k+1) = V_i(k) + \Delta V_i(k) \\ \omega_i(k+1) = \omega_i(k) + \Delta \omega_i(k) \\ \delta_i(k+1) = \delta_i(k) + \Delta \delta_i(k) \end{cases} \quad (6)$$

The network characteristics are constrained to be within specified boundaries:

$$\begin{cases} \underline{\omega} < \omega(k+1) < \overline{\omega} \\ \underline{V} < V_i(k+1) < \overline{V} \end{cases} \quad (7)$$

where \overline{X} and \underline{X} , are the maximum and minimum bounds of the variable X .

D. Power electronics interfaced generation

Based on the considered time scale, it is only relevant to capture the dynamics of the droop control. The conventional double-loop control (see [9] for a detailed description) are then neglected, and we refer to [10] for a complete review of the droop techniques. The main dynamics of the droop technique

are recalled in (8). We refer the set of droop-controlled nodes by \mathcal{N}_d , and for $i \in \mathcal{N}_d$,

$$\begin{cases} P_i^{gen}(k+1) - P_i^{gen-ref}(k+1) = -k_{pi} \cdot (\omega(k+1) - \omega^*) \\ Q_i^{gen}(k+1) - Q_i^{gen-ref}(k+1) = -k_{qi} \cdot (V_i(k+1) - V_i^*) \end{cases} \quad (8)$$

Equation (7) directly introduces the levers of the droop-controlled power electronic devices that are the active and reactive power references denoted by $P_i^{gen-ref}$ and $Q_i^{gen-ref}$, respectively. Finally, with

$$\begin{aligned} P_i^{gen-ref}(k+1) &= P_i^{gen-ref}(k) + \Delta P_i^{gen-ref}(k) \\ Q_i^{gen-ref}(k+1) &= Q_i^{gen-ref}(k) + \Delta Q_i^{gen-ref}(k) \end{aligned} \quad (9)$$

we obtain the following model of the droop-controlled inverters:

$$\begin{aligned} P_i^{gen}(k+1) &= P_i^{gen-ref}(k) + \Delta P_i^{gen-ref}(k) \\ &\quad - k_{pi} \cdot (\omega(k+1) - \omega^*) \\ Q_i^{gen}(k+1) &= Q_i^{gen-ref}(k) + \Delta Q_i^{gen-ref}(k) \\ &\quad - k_{qi} \cdot (V_i(k+1) - V_i^*) \end{aligned} \quad (10)$$

Although we could also use the voltage magnitude and the system frequency as lever, in the remainder, we discarded this possibility. Equation (8) contains an algebraic relation between two states $P_i^{gen}(k+1)$ and $\omega(k+1)$ that we can solve by reinjecting (6) into (10) the same hold for the reactive power and the voltage node. The last dynamics to include in the model is related to the storage capability and the state of charges. The storage devices are considered as ideal and can be represented as:

$$SoC_i(k+1) = SoC_i(k) - \eta_{ch} \frac{P_i^{gen}(k+1) \cdot Ts}{60} \quad (11a)$$

$$SoC_i(k+1) = SoC_i(k) - \eta_{disch} \frac{P_i^{gen}(k+1) \cdot Ts}{60} \quad (11b)$$

depending on if $P_i(k+1) < 0$ (11a) or $P_i(k+1) > 0$ (11b) with the following constraints:

$$\begin{aligned} SoC &< SoC(k+1) < \overline{SoC} \\ \underline{P_i^{gen}} &< P_b(k+1) < \overline{P_i^{gen}} \end{aligned}$$

E. Conventional generation

Conventional generators, such as diesel or gas generators are modelled as controlled power sources. The output active power and the apparent power are bounded and can be modelled as:

$$P_{gen}(k+1) = P_{gen}(k) + \Delta P_{gen}(k) \quad (12)$$

$$\begin{cases} P_{gen} < P_{gen}(k+1) < \overline{P_{gen}} \\ \sqrt{P_{gen}^2 + Q_{gen}^2} < S_{gen}^{\max} \end{cases}$$

F. Loads and renewable generations

For sake of simplicity, the renewables sources are modelled as negative loads. The supervisor will deal with the loads and renewables sources as known disturbances profiles from a forecast module. Finally, the optimization problem solved by the supervisor is formulated as a MIQP (Mixed Integer Quadratic Program):

$$\min_{\Delta u} \sum_{k=1}^{N_c} \left[\alpha(\tilde{y}(k) - y^*(k))^2 + \beta(\Delta u(k))^2 + \lambda(P_{los})^2 \right] \quad (13)$$

subject to the microgrid dynamics:

$$\begin{aligned} X(k+1) &= \mathbf{A}.X(k) + \mathbf{B}.\Delta U(k) + \mathbf{C}.\Delta D(k) \\ Y(k) &= \mathbf{C}.X(k) \end{aligned} \quad (14)$$

where the matrices \mathbf{A} , \mathbf{B} , \mathbf{D} and \mathbf{C} are obtained based on the linear model of each equipment, and the vector $X(k)$, $\Delta U(k)$ are defined as follows, and we denote the set of nodes, the set of droop-controlled nodes, and the set of controlled nodes by \mathcal{N} , \mathcal{N}_d , \mathcal{N}_p

$$X(k) = \begin{bmatrix} [SoC_{l \in \mathcal{N}_d}]^T \\ \omega \\ [V_{i \in \mathcal{N}}]^T \\ [\delta_{i \in \mathcal{N}}]^T \\ [P_{i \in \mathcal{N}}]^T \\ [Q_{i \in \mathcal{N}}]^T \\ [P_{j \in \mathcal{N}_p}^{gen_ref}]^T \\ [Q_{j \in \mathcal{N}_p}^{gen_ref}]^T \end{bmatrix} \quad \Delta U(k) = \begin{bmatrix} \Delta P_{j \in \mathcal{N}_p}^{gen_ref}(k) \\ \Delta Q_{j \in \mathcal{N}_p}^{gen_ref}(k) \end{bmatrix}$$

III. SIMULATION RESULTS

The proposed supervisor has been implemented in MATLAB with the toolbox YALMIP [11]. The solver used for the optimization problem is Gurobi. The model of the microgrid is depicted on Figure 10, and the specifications of the storage devices and PV systems are summarized in Table 2. The renewable and load forecasts for both simulation are also presented in Appendix. The reference case presents the microgrid without any physical representation of the microgrid lines. It represents the raw economic optimization and the state of Charge at the end of the day will serve as a reference to compare both supervisors. The results are presented in Figure 4. The final states of charge are 0.22 and 0.59.5 p.u for battery 1 and 2 respectively.

A. Case 1: Classical supervisor

The first simulation case only includes the tracking of the economical references. This simulation presents the conventional proposition for the microgrid secondary control. In this case, for every new economical reference, a power flow routine is computed to define the initial operating point and the matrices to generate the linear model embedded within the supervisor. The voltage set point is set to 1 p.u at the node 1. There is no change in references and the microgrid is only led by the initial set point from the economical optimization,

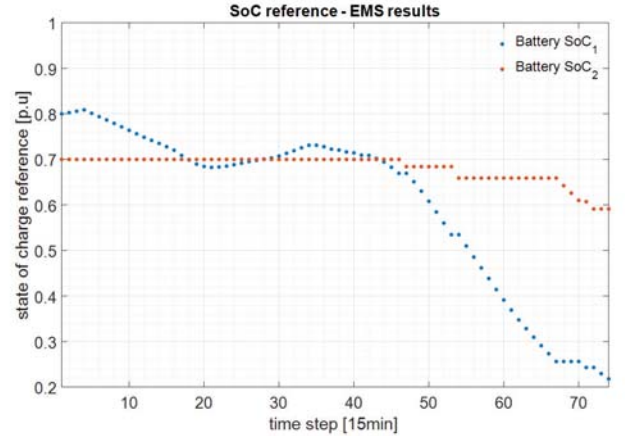


Fig. 4: Economical optimal SoC trajectory

unless voltage or frequency deviations exceed the limitations. This supervisor exhibits around 0.007 p.u of mean losses as shown in Figure 5. For the sake of clarity, we only present the voltage of the generators (batteries) and of the extremal nodes (nodes 15, 17, 18, cf. Figure 10). As expected, the voltage at the node 1 is close to 1 p.u, and the voltage and the extrema of the microgrid change up to 1.01 p.u when the renewable produces, and down to 0.97 p.u during the evening peak load. Figure 6 presents the daily power profile. At first, the battery

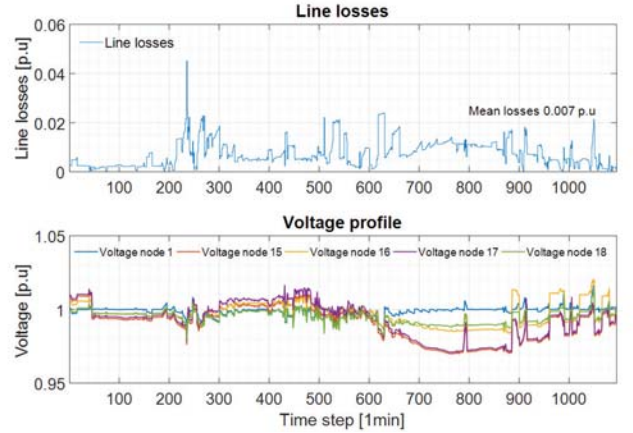


Fig. 5: Losses and voltage profile - case 1

1 is charged with the diesel generator (before 60 min) in order to store enough reserves in the storage devices for this day. Before 200 min, the power predictions are accurate enough so that the profile is very similar to the economical optimization expected values and only the battery at the node 1 supply the load. Fast fluctuations of the renewable 1 lead to a reaction of the droops of battery 1 and 2 as can be seen between 400 and 600 min. Finally, after 800 min, the state of charge of the battery 1 approaches its minimum and battery 2 is thus more called for. It can be noticed that the voltage is maintained within the specified limits (± 0.05 p.u) and the frequency between 0.01 p.u. Finally, with this supervisor, the final states of charge are 0.218 and 0.563 p.u.

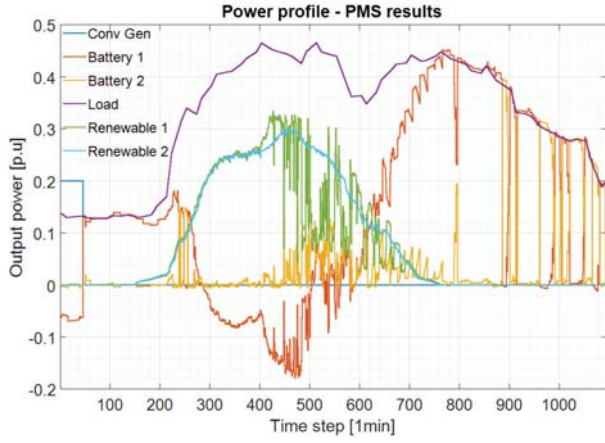


Fig. 6: Power profile - case 1

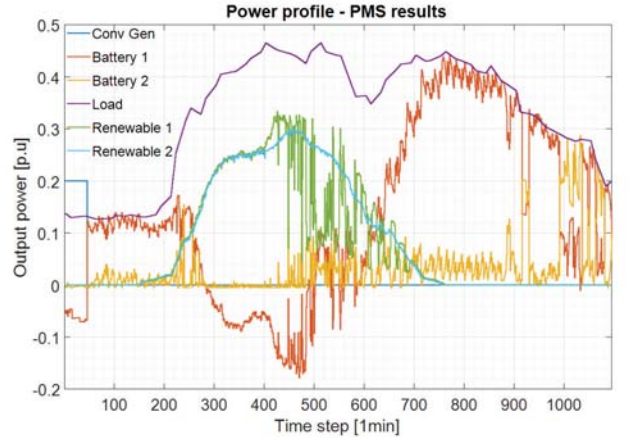


Fig. 8: Power profile - case 2

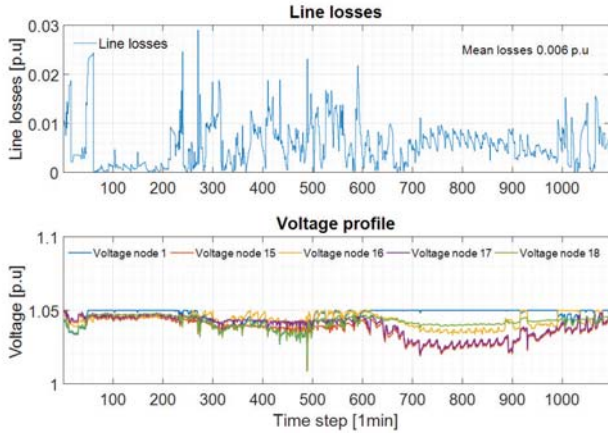


Fig. 7: Losses and voltage profile - case 2

B. Case 2: Novel supervisor

The second simulation presents the results of the tracking of the economical references while minimizing the line losses. With this supervisor, the losses are reduced to 0.006 p.u. It is worth noting that the weight of the line losses is relatively low in this case. As expected, the supervisor tends to increase the voltage to its upper bound and it can be observed some rapid changes of the voltage of the nodes 16, 17 and 18 due to the misleading references from the economical optimization, and the correction applied by the supervisor. It can be noticed that the supervisor is able to react to fast fluctuations of the renewable in order to maintain the voltage within the specified boundaries. Furthermore, in the microgrid, the ratio X/R is relatively low, and thus, to reduce the losses, the supervisor tends to use the active power references, as it can be seen in Figure 10 with the fluctuations of the output powers of both batteries. This lead to an opposite effect to the objective which is desired with the economical references tracking. Finally, with this supervisor, the final states of charge are 0.201 and 0.610 p.u.

C. Comparison

Table 1 presents the main results of both supervisors compared to the predicted optimal references. It can be noticed that in term of total energy the proposed supervisor is closer to the EMS. This represents a difference of about 9 kWh between both supervisors, and no differences compared to the purely economic references. In the first simulation, the position within the microgrid of the reserves of ESS2 is not respected as, due to its positioning, the second battery has been used to reduce the losses. However, with the proposed supervisor, the ESS1 is used to minimize the losses and mitigate to the fluctuations.

TABLE I: Performance comparison

Performances		EMS	PMS1	PMS2
State of charge [p.u]	ESS1	0.220	0.218	0.201
	ESS2	0.595	0.563	0.610
Losses [p.u]		-	0.007	0.006

Those two simulations demonstrate that the proposed supervisor can efficiently reduce the line losses without deteriorating the economic performance of the microgrid supervisor. This is achieved at the cost of power fluctuations to correct the misleading economical references. Finally, the proposed supervisor improves on the conventional one, but it is to be noted that the repartition of the available reserves is incorrect regarding what is expected from the economical point of view. This point may be a challenge if different storage devices exhibit different objectives, such as hydrogen storage for long term and lead-acid battery for instance for intra-day management. This point could be improved with a sensitivity analysis of the economical layer to improve the weighting factors used to minimize the losses.

IV. CONCLUSION

We proposed an improved supervisor that preserves the common three-layer structure of microgrid supervisor. It is able to track the economical references and takes advantage of the model embedded in the MPC to minimize the losses without performing a non-linear OPF at each time step. The simulations presented an improvement in the minimization of the losses at the cost of changes in active power references that may lead to errors in the economical tracking problem. The main perspectives are twofold. First, due to the linearization of the network model, the losses may not be correctly estimated. A comparison with successive optimal power flows may confirm this assumption. The computation time required to solve the non-linear optimal power flows. Secondly, the droop coefficient may also be used as a third lever to reduce the losses. It is expected that the closer to the fluctuations the storage devices, the higher the droop coefficient.

REFERENCES

- [1] Y. Han, H. Li, P. Shen, E. A. A. Coelho, and J. M. Guerrero, "Review of Active and Reactive Power Sharing Strategies in Hierarchical Controlled Microgrids," *IEEE Transactions on Power Electronics*, vol. 32, no. 3, pp. 2427–2451, 2017.
- [2] S. M. Zanolli and C. Pepe, "The importance of cooperation and consistency in two-layer Model Predictive Control," *Proceedings of the 2016 17th International Carpathian Control Conference, ICC 2016*, pp. 825–830, 2016.
- [3] B. Picasso, D. De Vito, R. Scattolini, and P. Colaneri, "An MPC approach to the design of two-layer hierarchical control systems," *Automatica*, vol. 46, no. 5, pp. 823–831, 2010.
- [4] S. Raimondi Cominesi, M. Farina, L. Giulioni, B. Picasso, and R. Scattolini, "Two-layer predictive control of a micro-grid including stochastic energy sources," *Proceedings of the American Control Conference*, vol. 2015-July, pp. 918–923, 2015.
- [5] P. Velarde, L. Valverde, J. M. Maestre, C. Ocampo-Martinez, and C. Bordons, "On the comparison of stochastic model predictive control strategies applied to a hydrogen-based microgrid," *Journal of Power Sources*, vol. 343, pp. 161–173, 2017.
- [6] P. Tatjewski, "Advanced control and on-line process optimization in multilayer structures," *IFAC Proceedings Volumes (IFAC-PapersOnline)*, vol. 11, pp. 13–26, 2007.
- [7] A. H. Fathima and K. Palanisamy, "Optimization in microgrids with hybrid energy systems - A review," *Renewable and Sustainable Energy Reviews*, vol. 45, pp. 431–446, 2015.
- [8] W. van Ackooij, I. Danti Lopez, A. Frangioni, F. Lacalandra, and M. Tahanan, "Large-scale unit commitment under uncertainty: an updated literature survey," *Annals of Operations Research*, vol. 271, no. 1, pp. 11–85, 2018.
- [9] M. Marwali and A. Keyhani, "Control of Distributed Generation Systems Part I: Voltages and Currents Control," *IEEE Transactions on Power Electronics*, vol. 19, no. 6, pp. 1541–1550, 2004.
- [10] M. Gutiérrez, T. Ixta, P. Zuniga, E. Barocio, and F. Uribe, "Droop controller comparison for AC microgrids," *2016 IEEE International Autumn Meeting on Power, Electronics and Computing, ROPEC 2016*, 2016.
- [11] J. Lofberg, "YALMIP : a toolbox for modeling and optimization in MATLAB," *2004 IEEE International Conference on Robotics and Automation (IEEE Cat. No.04CH37508)*, pp. 284–289, 2004.
- [12] K. Strunz, E. Abbasi, C. Abbey, C. Andrieu, U. Annakkage, S. Barsali, R. C. Campbell, R. Fletcher, F. Gao, T. Gaunt, A. Gole, N. Hatzigiorgiou, R. Iravani, G. Joos, H. Konishi, M. Kuschke, E. Lakervi, C.-C. Liu, J. Mahseredjian, F. Mosallat, D. Muthumuni, A. Orth, S. Papathanassiou, K. Rudion, Z. Styczynski, and S. C. Verm, "Benchmark Systems for Network Integration of Renewable Energy Resources," Tech. Rep. 273, 2014.

V. APPENDIX

TABLE II: DER Parameters

Type	Node	P_{nom} [kW]
ESS	1	100
ESS	16	100
PV	8	100
PV	11	100
Genset	5	100

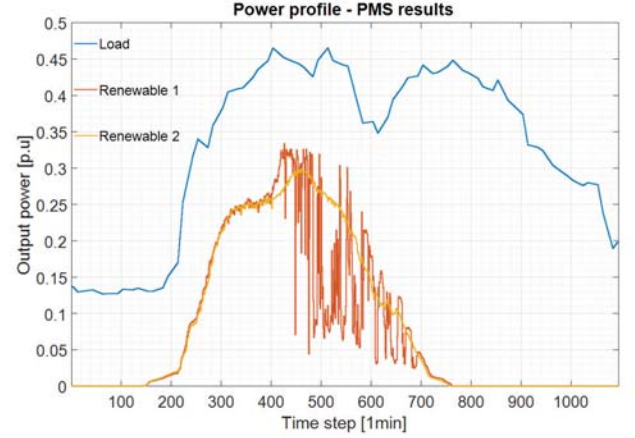


Fig. 9: PV and load power Profiles

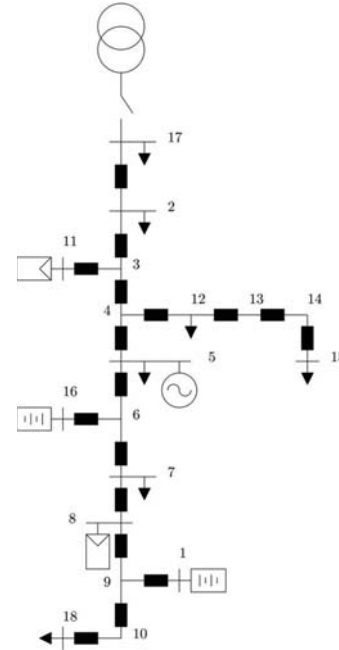


Fig. 10: Modified CIGRE European LV network testbench [12]